Published in final edited form as:
Cell Tissue Res. 2011 April ; 344(1): 17–30. doi:10.1007/s00441-011-1138-1.

Relationship between interstitial cells of Cajal, fibroblast-like cells and inhibitory motor nerves in the internal anal sphincter

Caroline A. Cobine, **Grant W. Hennig**, **Masaaki Kurahashi**, **Kenton M. Sanders**, **Sean M. Ward**, and **Kathleen D. Keef**
Department of Physiology and Cell Biology, University of Nevada School of Medicine, Reno, NV 89557, USA

Kathleen D. Keef: kkeef@medicine.nevada.edu

Abstract

Interstitial cells of Cajal (ICC) have been shown to participate in nitrergic neurotransmission in various regions of the gastrointestinal (GI) tract. Recently, fibroblast-like cells, which are positive for platelet-derived growth factor receptor α (PDGFRα$^+$), have been suggested to participate additionally in inhibitory neurotransmission in the GI tract. The distribution of ICC and PDGFRα$^+$ cell populations and their relationship to inhibitory nerves within the mouse internal anal sphincter (IAS) are unknown. Immunohistochemical techniques and confocal microscopy were therefore used to examine the density and arrangement of ICC, PDGFRα$^+$ cells and neuronal nitric-oxide-synthase-positive (nNOS$^+$) nerve fibers in the IAS of wild-type (WT) and *W/W^v* mice. Of the total tissue volume within the IAS circular muscle layer, 18% consisted in highly branched PDGFRα$^+$ cells (PDGFRα$^+$-IM). Other populations of PDGFRα$^+$ cells were observed within the submucosa and along the serosal and myenteric surfaces. Spindle-shaped intramuscular ICC (ICC-IM) were present in the WT mouse IAS but were largely absent from the *W/W^v* IAS. The ICC-IM volume (5% of tissue volume) in the WT mouse IAS was significantly smaller than that of PDGFRα$^+$-IM. Stellate-shaped submucosal ICC (ICC-SM) were observed in the WT and *W/W^v* IAS. Minimum surface distance analysis revealed that nNOS$^+$ nerve fibers were closely aligned with both ICC-IM and PDGFRα$^+$-IM. An even closer association was seen between ICC-IM and PDGFRα$^+$-IM. Thus, a close morphological arrangement exists between inhibitory motor neurons, ICC-IM and PDGFRα$^+$-IM suggesting that some functional interaction occurs between them contributing to inhibitory neurotransmission in the IAS.

Keywords

Gastrointestinal tract; Smooth muscle; Enteric; Immunohistochemistry; Morphology; Platelet-derived growth factor receptor α; Mouse

Introduction

Inhibitory neuromuscular transmission in the gastrointestinal (GI) tract involves multiple neurotransmitters including nitric oxide (NO), purines such as ATP and peptides such as vasoactive intestinal polypeptide (Burnstock 2008). Evidence has been presented that each of these putative neurotransmitters contributes to inhibitory motor innervation in the mouse

Correspondence to: Kathleen D. Keef, kkeef@medicine.nevada.edu.

Electronic supplementary material The online version of this article (doi:10.1007/s00441-011-1138-1) contains supplementary material, which is available to authorized users.

internal anal sphincter (IAS; McDonnell et al. 2008; Rattan 2005). In spite of these multiple pathways, a general consensus exists that each class of neurotransmitter is probably released from the same population of inhibitory nerve fibers (Burnstock 2008). Thus, the identification of the location of neuronal nitric oxide synthase (nNOS) might also provide some general insight into the distribution of inhibitory motor neurons.

The simplest scheme for motor innervation is the direct innervation of smooth muscle cells (SMC) by motor nerve endings. However, evidence has revealed that innervation in the GI tract is more complicated. In addition to SMC connecting to one another via gap junctions, two other cell types have been shown to connect via gap junctions to SMC (Horiguchi and Komuro 2000; Komuro 1999) and these cells might contribute to receiving and transducing motor neurotransmitter signals. For example, evidence has suggested that interstitial cells of Cajal (ICC) participate in nitrergic neurotransmission in GI muscles (Burns et al. 1996; Sanders et al. 2010; Ward and Sanders 2006); however, controversy exists about the role of ICC in nitrergic responses (Goyal and Chaudhury 2010; Huizinga et al. 2009). ICC do not appear to be necessary for purinergic transmission, as this pathway persists in stomachs and lower esophageal sphincters of mutant animals lacking ICC (Sergeant et al. 2002; Ward et al. 1998; Zhang et al. 2010). Recent studies have implicated cells termed fibroblast-like cells as participants in purinergic transmission in the GI tract (Kurahashi et al. 2011; Klemm and Lang 2002). These cells have morphological features characteristic of fibroblasts and can be clearly distinguished from SMC and ICC in GI muscles by electron microscopy (Zhou and Komuro 1992; Horiguchi and Komuro 2000). Fibroblast-like cells within the muscularis are associated with nerves (Komuro 1999) and recent studies have shown that these cells express small-conductance calcium-activated potassium channels, SK3 (Kcnn3) and P2Y1 (P2ry1) receptors, both of which are critical for purinergic neurotransmission (Vanderwinden et al. 2002; Iino and Nojyo 2009; Klemm and Lang 2002; Fujita et al. 2003; Kurahashi et al. 2011). A recent study has also reported that fibroblast-like cells can express guanylate cyclase, the postjunctional receptor for nitric oxide (Iino et al. 2008) and so these cells might also be responsive to nitrergic signals. Fibroblast-like cells have attracted additional interest bcause of their persistence in animal models lacking ICC (Farre et al. 2007; Iino et al. 2008; Vanderwinden et al. 2002; Horiguchi and Komuro 2000). The morphology of ICC and fibroblast-like cells and their relative anatomical proximity to inhibitory motor neurons in the IAS is unknown.

In the present study, we have examined the morphology and distribution of ICC and fibroblast-like cells in the mouse IAS and their relationships of these cells to $nNOS^+$ nerve fibers in WT mice and in $Kit^{W/Wv}$ (W/W^v) mice, in which ICC numbers are greatly reduced in many regions of the GI tract. ICC have been identified by immunolabeling with antibodies against KIT (Ward et al. 1994). Fibroblast-like cells have been identified by immunolabeling the receptor tyrosine kinase, platelet-derived growth factor receptor α (PDGFRα), which has been shown to be highly specific for fibroblast-like cells (Kurahashi et al. 2011; Iino et al. 2009a). We have also used the *Pdgfra*$^{tm11(eGFP)Sor}$*/J* heterozygote mouse (Hamilton et al. 2003), which expresses enhanced green fluorescent protein (eGFP) in $PDGFR\alpha^+$ cells (Kurahashi et al. 2011), as an additional tool to examine the distribution of fibroblast-like cells. ICC, $PDGFR\alpha^+$ cells and neural processes expressing nNOS (i.e., inhibitory motor neurons) have been identified throughout the muscularis of the IAS and the morphological features, volume distributions and associations with other cell types have been quantified. We have found significant spatial alignment between all three cell types in the IAS, suggesting that intramuscular $PDGFR\alpha^+$ cells ($PDGFR\alpha^+$-IM) and intramuscular ICC (ICC-IM) contribute to the inhibitory neuromuscular control of IAS tone.

Materials and methods

Tissue preparation

The animals used for these studies were maintained and the experiments performed in accordance with the National Institutes of Health Guide for the Care and Use of Laboratory Animals and the Institutional Animal Use and Care Committee at the University of Nevada approved all procedures used.

C57BL/6, *W/W*^{v} and *Pdgfra*$^{tm11(eGFP)Sor}$*/J* heterozygote mice (30–90 days old; Jackson Laboratory, Bar Harbor, Me., USA) were killed with isoflurane (Baxter, Deerfield, Ill., USA) followed by cervical dislocation. The rectoanal region was removed by cutting through the pelvic bone and spine with scissors and dissecting away overlying tissue.

Rectoanal segments (15 mm) were mounted in a dissection dish containing cold Krebs bicarbonate solution (KRBS) of the following composition: 118.5 mM NaCl, 4.7 mM KCl, 2.5 mM$CaCl_2$, 1.2 mM $MgCl_2$, 23.8 mM$NaHCO_3$, 1.2 mM KH_2PO_4, 11.0 mM dextrose. This solution had a pH of 7.4 at 37°C when bubbled to equilibrium with 95% O_2, 5% CO_2. For whole-mount immunohistochemistry, the GI tract was cut open and pinned flat and all adhering skeletal muscle, glands and mucosa were dissected away.

Light microscopy

The overall morphology of the mouse rectoanal region was examined by preparing 3-mm-thick cross sections of the rectoanal region with the external anal sphincter (EAS) and mucosa left attached. Muscle preparations were fixed in 4% (wt/vol) ice-cold paraformaldehyde in a 0.1 M phosphate buffer solution (PBS) at 4°C overnight. Muscles were subsequently dehydrated and embedded in paraffin wax. Sections (10 μm) were cut and then stained with Masson's Trichrome and examined with a Nikon Eclipse E800 microscope (Nikon, USA). Photomicrographs were acquired by using a Spot RT Slider charge-coupled device camera (Diagnostic Instruments, Mich., USA) with proprietary software.

Whole-mount immunohistochemistry

Rectoanal whole-mount preparations were fixed for 15 min with either ice-cold paraformaldehyde (4% w/v) or ice-cold acetone. Tissues were then washed in 0.1 M PBS overnight at 4°C. To reduce non-specific antibody binding, tissues were preincubated in bovine serum albumin (BSA; 1% w/v for 1 h at 20°C; Sigma, St. Louis, Mo., USA) before incubation with the first primary antibody. To achieve greater penetration during labeling, incubations of the tissue preparations with the primary antibodies were carried out by using Triton-X 100 (0.5%; Sigma). Incubation with the first primary antibody was carried out for 48 h at 4°C. Following 5–6 h of washing in PBS, tissues were incubated with the corresponding secondary antibody (Molecular Probes, Eugene, Ore., USA) for 1 h at 20°C. Tissues were washed in 0.1 M PBS overnight at 4°C. Whole-mount preparations were then incubated in BSA (1% w/v) for 1 h at 20°C before incubation with the second primary antibody for 48 h at 4°C. Tissues were washed for 5–6 h in PBS and incubated with the corresponding secondary antibody (Molecular Probes) at a working dilution of 1:1000 for 1 h at 20°C. Tissues were washed overnight at 4°C before being mounted on glass slides with coverslips by using Aquamount mounting medium (Lerner Laboratories, Pittsburgh, Pa., USA).

Identification of PDGFRα-eGFP^{+} cells and calculation of cell number

Pdgfra$^{tm11(eGFP)Sor}$*/J* heterozygote mouse ring preparations were made by removing all adhering skeletal muscle and glands whilst keeping the tubular structure of the rectoanal

region intact; 2-mm-wide rings of IAS and rectum were prepared and then fixed for 15 min with ice-cold paraformaldehyde at 20°C. Tissues were then washed in 0.1 M PBS overnight at 4°C, dehydrated in graded sucrose solutions (5%, 10%, 15%for 15 min each and 20%overnight) before being embedded in a 1:1 solution of Tissue Tek OTC compound (Sakura Finetek, Torance, CA) and 20% sucrose and stored at −80°C. Sections were cut transverse to the circular muscle (CM) layer at a thickness of 10–12 μm (thin sections) by using a Leica CM 3050 cryostat (Leica Microsystems, Wetzlar, Germany). To reduce non-specific antibody binding, tissues were incubated in BSA (1% w/v for 1 h at 20°C; Sigma) before incubation with PDGFRα antibody (R&D Systems, Minneapolis, Minn., USA) in combination with Triton-X 100 (0.5%solution for 16 h at 4°C). Slides were washed in PBS (0.1 M for 6 h) and then incubated with the corresponding secondary antibody (Molecular Probes) at a working dilution of 1:1000 (1 h at 20°C). The unbound secondary antibody was removed by washing the slides in PBS overnight. Cells within the tissue preparation were counterstained with 4,6-diamidino-2-phenylindole (DAPI) by using Vectashield DAPI mounting medium (Vector Laboratories, Burlingame, Calif., USA) and then cover-slipped. eGFP-positive cells that were also PDGFRα$^+$ were counted within the CM layer of 10-μm-thick confocal stacks. The total cell number within the CM was calculated by counting the number of cells counterstained with DAPI. Cells that were both eGFP-positive and PDGFRα$^+$ were then expressed as a percentage of the total cell number.

Imaging

A Zeiss LSM 510 Meta confocal microscope (Carl Zeiss, Thornwood, NY) was used to examine immunohistochemically labeled specimens. Micrographs of whole-mount specimens, generated by using the confocal imaging system, were prepared from digital composites of a Z-series of scans of 0.25–1 μm optical sections through a depth of 0.5–35 μm. Final images were constructed by using Zeiss LSM 5 Image Examiner Software, Adobe Photoshop CS2 Software and CorelDRAW X3 Software. DAPI images were acquired with an Olympus FluoView FV1000 confocal microscope (Olympus Corporation, Tokyo, Japan) and images were constructed by using Olympus FluoView Ver.2.1a Software, Adobe Photoshop CS2 and CorelDRAW X3 Software. Immunoreactivity was detected with secondary antibodies conjugated with either Alexa Fluor 594 (KITand PDGFRα, red) or Alexa Fluor 488 (PDGFRα and nNOS, green).

In most images, ICC and PDGFRα$^+$ cells are shown in color. However, in some images, the labeling has been converted to reverse grayscale by using Adobe Photoshop. In Supplementary Fig. 2, the contrast between PDGFRα, DAPI and eGFP has been enhanced by selecting all red pixels in each image and assigning them a brighter red color by means of Photoshop (Adobe, Mountain View, Calif., USA).

Controls

To ensure the specificity of the labeling, control tissues were examined. These were prepared by omitting either the primary or secondary antibodies from the incubation solutions. Single-labeled tissue specimens were also prepared to confirm the specificity of the antibodies in double-label experiments. For most ICC labeling, the KIT antibody mSCFR was used (including the images shown in the figures). The specificity of this labeling was further examined by using a second anti-KIT antibody (i.e., ACK2, see Table 1). Additionally, two different PDGFRα antibodies were used. Cells identified in both cases had the same morphology and distribution as the ICC (KIT) or fibroblast-like cells (PDGFRα) observed with the other antibody.

Volume and alignment analysis

Confocal stacks were processed (smoothed by using a 0.6 μm box filter) and thresholded and a marching cubes algorithm was applied (Volumetry G7mv, GWH). The volume was calculated, the non-surface coordinates were discarded and the remaining surface triangles were smoothed twice by using a Laplacian "shrink-expand" algorithm (lambda 0.35, 0.1, respectively) that better preserved the volume of structures. The surfaces of two different cell types were then compared by randomly selecting 15,000 surface coordinates from one cell type and then searching the entire surface coordinates of the other cell type to find the closest point (absolute μm). Histograms were constructed to show the frequency of the minimum distances between the models (0–14 μm). To examine the alignment of two cell types, the surface coordinated from one cell type was rotated by 90 degrees and the minimum surface distance analysis repeated. No change in the minimum surface distance histograms indicated that the two cell types had no preferential alignment with each other and vice versa. Three-dimensional models were rendered after the addition of surface normals to display lighting effects. Anaglyphs were prepared by introducing a pixel offset related to the depth of the slice in the confocal stack (see Cobine et al. 2010a for a full explanation).

Statistics

Data are expressed as mean±SE and values were considered significantly different when $P<0.05$. Each image was assigned an n value of one and labeling experiments were repeated on muscles from a minimum of at least two animals.

Results

Morphology of mouse IAS

The gross morphology of the murine rectoanal region was examined with Masson's Trichrome staining techniques. The IAS was composed of longitudinal muscle (LM) and CM layers. The CMwas thicker than the LM layer (100 μmvs. 40 μm, Fig. 1a−c) and extended more distally than the LM layer. A band of connective tissue containing non-muscle cells and enteric neurons was present between the LM and CM layers. More distinct septa separated muscle into bundles in the IAS than in the rectum (Fig. 1c, d). The EAS, composed of skeletal muscle, was located at the distal extremity and overlapped the IAS to a limited extent (Fig. 1a, b). Glands were also observed between the IAS and EAS and sometimes separated the two sphincters (Fig. 1a, c).

Morphology and distribution of ICC in IAS of wild-type and *W/W^v* mice

The morphology and distribution of ICC in the IAS of wild-type (WT) and *W/W^v* mice were characterized by immunofluorescence by using anti-KIT antibodies in whole-mount preparations. Two distinct populations of ICC were observed in WT mice. ICC-IM were spindle-shaped and found within muscle bundles in the LM and CM (Fig. 2a, c, Supplementary Fig. 1a). ICC were also found distributed along the submucosal surface of the CM (ICC-SM). These cells were extensively branched and found in clusters, rather than forming a distinct network (Fig. 2d, e). In contrast to most of the GI tract, we did not observe a network of cells in the space between the CM and LM in the IAS (i.e., myenteric ICC or ICC-My; Fig. 2b). ICC-SM were present in *W/W^v* mice (Fig. 2f) but, in contrast to WT mice, ICC-IM were largely absent (Fig. 2g).

Relationship of nNOS$^+$ nerve fibers to ICC

The relationship of nNOS$^+$ nerve fibers to ICC was characterized in WT and *W/W^v* mice by dual-labeling muscles with anti-KIT and anti-nNOS antibodies in whole-mount

preparations. A plexus of nNOS$^+$ neurons and processes were present at the myenteric plexus (Fig. 3c, f, Supplementary Fig. 3c, f), whereas nerve processes formed a plexus at the submucosal surface and cell bodies were rare (Fig. 3a, d, Supplementary Fig. 3a, d). Within the muscularis, nNOS$^+$ nerve fibers ran parallel to the long axis of SMC in the CM (Fig. 3b, e, Supplementary Fig. 3b, e). In WT mice, some ICC-IM were closely associated with nNOS$^+$ nerve fibers (Fig. 3b, g). ICC-IM were largely absent in *W/W^v* mice but nNOS$^+$ nerve fibers were present in an equivalent density to that in WT mice (Fig. 3e). ICC-SM were present in WT and *W/W^v* mice (Fig. 3a, d). ICC-IM volume, as a percent of tissue volume, was approximately equal to the volume of nNOS$^+$ cell processes (i.e., 5.4±0.6%, *n*=5, versus 5.3±0.7%, *n*=5, of total CM volume).

Morphology and distribution of PDGFRα$^+$ cells in WT, *W/W^v* and *Pdgfra$^{tm11(eGFP)Sor}$/J* heterozygote mice

The morphology and distribution of PDGFRα$^+$ cells were examined in whole-mount preparations of WT and *W/W^v* mouse IAS (Fig. 4). PDGFRα$^+$ cells were found within muscle bundles of the CM and LM (PDGFRα$^+$-IM), within the region of the myenteric plexus (PDGFRα$^+$-My), along the serosal surface (PDGFRα$^+$-SS) and within the submucosa (PDGFRα$^+$-SM). PDGFRα$^+$-IM were highly branched and generally oriented in the long axis of SMC in the LM (Fig. 4a) and CM (Fig. 4b, Supplementary Fig. 1b) layers. PDGFRα$^+$-My (Fig. 4c), PDGFRα$^+$-SM (Fig. 4d) and PDGFRα$^+$-SS (Fig. 4e) were also branched but had fewer secondary branches and larger cell bodies. The orientation of these cells was more random than that of PDGFRα$^+$-IM. No obvious difference was observed in the PDGFRα$^+$ cell morphology and distribution in the *W/W^v* mouse IAS (e.g., Fig. 4f).

The density of PDGFRα$^+$ cells was examined in *Pdgfra$^{tm11(eGFP)Sor}$/J* heterozygote mice. In these mice, cells that express PDGFRα also express a histone 2B-eGFP fusion protein limiting eGFP expression to the nucleus (Hamilton et al. 2003). This nuclear expression provides a convenient means for counting total cell numbers. eGFP-positive nuclei were distributed throughout the musculature of the IAS at a density of approximately 300,000 cells/mm^3 within the CM layer (Fig. 5a). Immunohistochemical techniques were used to confirm that eGFP$^+$ cells did indeed express PDGFRα (Fig. 5b, c, Supplementary Fig. 2). All nuclei were also identified with the DNA counterstain DAPI. By comparing eGFP-positive cells with the total number of cell nuclei, we estimated that PDGFRα$^+$-IM represented approximately 25±2.3% (*n*=7) of the total cell number within the CM layer (Fig. 5b, c).

Relationship of nNOS$^+$ nerve fibers to PDGFRα$^+$ cells

The relationship of nNOS$^+$ nerve fibers to PDGFRα$^+$ cells in the IAS of WT and *W/W^v* mice was compared by dual-labeling tissues with anti-nNOS and anti-PDGFRα antibodies in whole-mount preparations. PDGFRα$^+$ cells formed a network along the submucosal (PDGFRα$^+$-SM) and myenteric (PDGFRα$^+$-My) surfaces but a high degree of close association was not noted between nNOS$^+$ nerve fibers and these cells (WT Fig. 6a, c; *W/W^v* Fig. 6d, f). Within the muscularis, however, all nNOS$^+$ nerve fibers were closely associated with PDGFRα$^+$-IM (Fig. 6b, g). The distribution of PDGFRα$^+$-IM and nNOS$^+$ nerve fibers and the close associations between these cells were similar in WT and *W/W^v* mice (Fig. 6b, e, g). Volume analysis revealed that the PDGFRα$^+$-IM volume was 2.7× that of nNOS$^+$ nerve fibers within the CM (i.e., 18.7±2.7%, *n*=5 versus 5.4±0.6%, *n*=5).

Relationship of ICC to PDGFRα$^+$ cells

Since ICC-IM and PDGFRα$^+$-IM were aligned with nNOS$^+$ nerve fibers, we undertook additional experiments to determine whether ICC-IM and PDGFRα$^+$-IM were also closely associated with one another. To determine the alignment between ICC-IM and PDGFRα$^+$-

IM, duallabeling experiments were performed. These data revealed an intimate morphological relationship between ICC-IM and PDGFRα$^+$-IM in the CM and LM (Fig. 7a, b). Interestingly, volume analysis revealed that PDGFRα$^+$-IM occupied 2.8× the volume of ICC-IM (i.e., 15.26±2.73%, *n*=5 versus 5.50±0.81%, *n*=5). In contrast, PDGFRα$^+$-SM were not closely associated with ICC-SM (Fig. 7c). PDGFRα$^+$-My were abundant in the myenteric region between CM and LM but ICC-My were not present (Fig. 7d), as described above. Along the serosal surface, small rounded KIT$^+$ cells with morphological features of mast cells were present but PDGFRα$^+$-SS were not associated with these cells (Fig. 7e).

Association of ICC-IM, PDGFRα$^+$-IM and nNOS$^+$ nerve fibers

The relationship between ICC-IM, PDGFRα$^+$-IM and nNOS$^+$ nerve fibers was further evaluated by utilizing a minimum distance surface algorithm to determine the minimum distance between the surfaces of the various cell types. This technique is obviously limited by the use of fluorescence but the analysis provides a statistically relevant comparison of distance between structures. To perform this analysis, cell surfaces were first rendered as described in Materials and methods and shown in Fig. 8a, Supplementary Fig. 4. Minimum distance analysis of nNOS and KIT or PDGFRα revealed that the greatest proportion of surfaces were located≤1 μm from each other. An exponential decline was seen in the proportion of surfaces located at greater distances (Fig. 8b). Interestingly, the surface relationships obtained for KIT/nNOS versus PDGFRα/nNOS were virtually identical, whereas ICC-IM with PDGFRα$^+$-IM had an even closer relationship (Fig. 8b). To examine whether different combinations of cell types were preferentially aligned in the same axis, one of the surface models was rotated 90° with respect to the other and the minimum surface distance analysis was repeated. Although the proportion of surfaces located at smaller distances declined for all cell combinations (KIT/nNOS, PDGFRα/nNOS, PDGFRα/KIT, Supplementary Fig. 5a−c), the steepest decline was seen with PDGFRα/KIT, indicating that these cells were preferentially aligned with one another along the CM axis (see Supplementary Fig. 5c).

Discussion

The present study describes the morphology and distribution of two classes of interstitial cells, viz., PDGFRα$^+$ cells and ICC, in the murine IAS and their relationship to nitrergic nerves in WT and *W/W^v* mice. Our data show that PDGFRα$^+$ cells are a significant component of the cellular mass of IAS muscles and are densely distributed from the submucosal to the serosal surfaces of the tunica muscularis. PDGFRα$^+$ cells are closely associated with ICC-IM and nNOS$^+$ nerve fibers and the relationship between PDGFRα$^+$ cells and motor nerve processes does not change significantly in *W/W^V* animals in the absence of ICC-IM. ICC-IM and PDGFRα$^+$ cells form gap junctions with SMC in GI muscles (Horiguchi and Komuro 2000; Komuro 1999) and both types of interstitial cells have been linked to transduction of inhibitory neurotransmitters in other regions of the gut (Burns et al. 1996; Kurahashi et al. 2011). Thus, PDGFRα$^+$ cells, ICC and SMC might constitute a triad of postjunctional cells, expressing receptors for neurotransmitters, transducing neural inputs and generating enteric inhibitory neural responses in the IAS. The way that these cells change during aging, diabetes and other disease states associated with fecal incontinence could provide new hypotheses concerning the etiology of IAS dysfunction.

PDGFRα is a receptor tyrosine kinase commonly expressed by fibroblasts in various organs (Betsholtz 2004; Bonner 2004). Previous studies have shown that PDGFRα is expressed in the muscularis during development and is critical for the development of LM (Kurahashi et al. 2008). Expression recedes once the LM is formed and adult animals retain a level of expression resolvable with immunofluorescence only in specific types of interstitial cells,

known previously by the vague term, fibroblast-like cells. Recent studies of GI muscles, from esophagus to rectum, have shown that PDGFRα is expressed by fibroblast-like cells (Iino and Nojyo 2009; Kurahashi et al. 2011). Our data showing that eGFP, driven from the endogenous PDGFRα promoter (Hamilton et al. 2003), is also confined to cells labeled with PDGFRα antibodies, further supports the conclusion that immunolabeling via PDGFRα is selective for these interstitial cells. We have suggested the replacement of the term "fibroblast-like cells" with PDGFRα$^+$ cells (Kurahashi et al. 2011; Sanders et al. 2010), in order clearly to distinguish this class of interstitial cells and the utilization of sub-classifications based on anatomical localization (e.g., PDGFRα$^+$-IM and PDGFRα$^+$-SM) as commonly used to distinguish the different types of ICC.

PDGFRα$^+$ cells are a major cellular phenotype in IAS. These cells are distributed throughout the IAS at an average volume density of ~300,000/mm^3 within the CM, representing about 25% of the total cell population. As discussed above, their consistent proximity suggests that they have some role in neurotransmission, as neuro-modulators, or in the maintenance of neuromuscular structures.

PDGFRα$^+$ cells appear at several general anatomical positions in the IAS including: (1) PDGFRα$^+$-SM in the submucosal region; (2) PDGFRα$^+$-IM within bundles of SMC of the CM and LM; (3) PDGFRα$^+$-My in the myenteric region between the CM and LM; (4) PDGFRα$^+$-SS at the serosal surface of the tunica muscularis. These cells differ in their morphology depending upon their location. PDGFRα$^+$-IM have several processes arising from a central nuclear area, together with numerous secondary branches, whereas PDGFRα$^+$-SM, PDGFRα$^+$-SS and PDGFRα$^+$-My have larger cell bodies, less branching and cells are distributed in a more random fashion. These differences in morphology (and differences in cell associations with neurons and ICC) suggest differences in function; however, this question will require future studies once means to isolate the specific classes of PDGFRα$^+$ cells are developed. Interestingly, although we have observed similar expression levels of PDGFRα in the submucosa and within the muscularis, only weak labeling of PDGFRα$^+$-SM has been reported elsewhere in the murine GI tract (Iino and Nojyo 2009). Thus, even PDGFRα$^+$ cells located within a particular structure (e.g., the submucosa) might differ between regions in the GI tract. Of interest to note, PDGFRα$^+$ cells differ structurally from ICC in the same anatomical niches. For example, PDGFRα$^+$-IM display several processes arising from a central nuclear area and numerous secondary branches, whereas ICC-IM are long thin spindle-shaped cells with few or no obvious processes. The differences in morphology between PDGFRα$^+$ cells and ICC, together with the lack of overlap between cells labeled with antibodies against PDGFRα$^+$ and KIT, support the conclusion that the two interstitial cells are distinct cell phenotypes.

Previous studies have identified ICC in the mouse IAS (de Lorijn et al. 2005; Terauchi et al. 2005) but the present study has extended this work by describing the specific locations of ICC within the tunica muscularis and by describing the lesion in ICC found in the IAS in *W/W^v* mice. ICC-IM, the major class of ICC within the IAS, are spindle-shaped and non-branching, as mentioned above. The morphology of the ICC-IM in the mouse differs from this class of ICC in the IAS of cynomolgus monkeys, where the IAS is subdivided into numerous "minibundles" and each minibundle contains clusters of highly branched ICC-IM (Cobine et al. 2010a). In the mouse, branching ICC are restricted to the submucosal surface (ICC-SM) where they were sparsely distributed. We have previously postulated that the ICC-IM serve as pacemaker cells in the monkey IAS. The ICC-SM possibly perform a similar function in the mouse IAS. The differences in ICC morphology and distribution between species might be attributable to the large difference in scale between them, i.e., the CM layer of the mouse IAS is approximately 1/20th the thickness of that of the cynomolgus monkey IAS. Thus, the CM layer of the mouse IAS is closer in size to a single "minibundle"

of the monkey IAS. The CM layer of the mouse IAS may therefore function more as a "single unit" type muscle with pacemaking arising from a single surface, whereas in the CM layer of the monkey (and dog), pacemaking is distributed throughout the muscle layer (Cobine et al. 2010a; Mutafova-Yambolieva et al. 2003). A similar distributed model of pacemaking has also been described for the guinea pig gallbladder (Lavoie et al. 2007) and the rabbit urethra (Hashitani and Suzuki 2007).

Although the ICC-IM differ between the mouse and monkey IAS, these muscles resemble one another in that both lack a network of ICC-My. Electrical slow waves are present in both species (Cobine et al. 2010b; Harvey et al. 2008) but unlike the small intestine in which slow waves arise from ICC-My (Lee et al. 2007), this class of ICC is not available for pacemaking in the IAS. In the mouse colon, ICC-SM have been shown to generate slow waves (Yoneda et al. 2004) and these ICC may serve a similar function in the murine IAS. The finding that slow waves (Cobine et al. 2010b) and ICC-SM (present study) persist in the W/W^v mouse suggests, as discussed above, that slow waves are generated by ICC-SM.

The organization of $nNOS^+$ nerves in the IAS is similar to that of the large intestine (Sang and Young 1996) including a plexus of nerve fibers at the myenteric and submucosal surfaces and varicose nerve fibers running parallel to SMC within the musculature. Also in agreement with previous studies (de Lorijn et al. 2005), no obvious differences exist in the distribution of nerves in WT and W/W^v mice.

$nNOS^+$ nerve fibers are closely associated with ICC and $PDGFR\alpha^+$ cells as demonstrated by our dual-labeling experiments. Minimum distance analysis has shown that surfaces of the interstitial cells and $nNOS^+$ nerve fibers are frequently≤1 μm from each other. Of course, fluorescence imaging does not allow the identification of close connections, such as synaptic contacts (Ward and Sanders 2006), since the maximum resolution is in the order of 0.3–0.8 μm with a 63× oil immersion objective having a numerical aperture of 1.4 (www.olympusconfocal.com/theory/resolutionintro.html). When minimum distance analysis is performed for ICC-IM versus $PDGFR\alpha^+$ cells, an even greater degree of alignment is seen (see above details of this analysis). The close association of ICC-IM and $PDGFR\alpha^+$-IM is also clearly visualized in the three-dimensional surface rendering shown in Fig. 8a, Supplementary Fig. 4. Previous studies of the GI muscles of mice (Iino and Nojyo 2009; Iino et al. 2009b; Rumessen and Thuneberg 1982; Vanderwinden et al. 2000; Kurahashi et al. 2011), human (Rumessen and Thuneberg 1991; Vanderwinden et al. 1999, 2000) and rat (Wang et al. 2009) have also revealed a close association between ICC and fibroblast-like cells and ultrastructural studies have shown that fibroblast-like cells are coupled to SMC via gap junctions (Horiguchi and Komuro 2000; Farre et al. 2007). Thus, ICC-IM and $PDGFR\alpha^+$-IM might each form part of the postjunctional apparatus that responds to neurotransmitter release and generates the junctional currents that are conducted to SMC. In a recent study, $PDGFR\alpha^+$ cells in the murine colon have been reported to express P2Y1 receptors and SK3 channels and to generate large Ca^{2+}-activated apamin-sensitive K^+ currents in response to purines (Kurahashi et al. 2011; Vanderwinden et al. 2002; Iino and Nojyo 2009). Thus, $PDGFR\alpha^+$ cells have the molecular and ionic apparatus to mediate purinergic neurotransmission. $PDGFR\alpha^+$ cells have also been shown to express guanylate cyclase (Iino et al. 2008), the receptor for NO, in some regions of the GI tract. Therefore, they might be involved in mediating nitrergic neurotransmission. Inhibitory neuromuscular transmission in the mouse IAS includes nitrergic and purinergic components (de Lorijn et al. 2005; McDonnell et al. 2008) and both ICC-IM and $PDGFR\alpha^+$-IM might participate in some aspects of transmission via these pathways.

Studies in the W/W^v mouse have revealed that ICC are also involved in cholinergic neurotransmission in the gastric fundus (Ward et al. 2000). Although no evidence is

currently available to suggest that PDGFRα$^+$ cells are involved in excitatory neurotransmission, they might also play a role in cholinergic transmission, given their close association with nerves and ICC. Further studies are required to examine this possibility.

In summary, this study describes the distribution of PDGFRα$^+$ cells and ICC in the murine IAS and their relationships to each other and to nitrergic nerves in WT and *W/W^v* mice. Our results show that PDGFRα$^+$ cells are densely distributed throughout the tunica muscularis and are closely associated with ICC-IM and nNOS$^+$ nerve fibers (Fig. 9). The morphology suggests that a functional relationship may exist between interstitial cells and inhibitory motor neurons that contributes to enteric inhibitory neuromuscular transmission. Future studies are required to evaluate this possibility and to address the changes that occur in the electrical and contractile events associated with nitrergic, purinergic and peptidergic transmission in the IAS of the *W/W^v* mouse, a model in which ICC-IM are largely absent.

Supplementary Material

Refer to Web version on PubMed Central for supplementary material.

Acknowledgments

The authors acknowledge the following individuals for their technical assistance with this work: Maria Durazo (Nevada State Health Laboratory), Byoung Koh, and Yulia Bayguinov.

This work was supported by grants DK078736 to K.D.K., DK057236 to S.M.W. and COBRE P20RR018751 to G.W.H. and by grant PPG DK41315. Imaging analysis was performed in a Core laboratory supported by P20RR018751.

References

Betsholtz C. Insight into the physiological functions of PDGF through genetic studies in mice. Cytokine Growth Factor Rev. 2004; 15:215–228. [PubMed: 15207813]

Bonner JC. Regulation of PDGF and its receptors in fibrotic diseases. Cytokine Growth Factor Rev. 2004; 15:255–273. [PubMed: 15207816]

Burns AJ, Lomax AE, Torihashi S, Sanders KM, Ward SM. Interstitial cells of Cajal mediate inhibitory neurotransmission in the stomach. Proc Natl Acad Sci USA. 1996; 93:12008–12013. [PubMed: 8876253]

Burnstock G. The journey to establish purinergic signalling in the gut. Neurogastroenterol Motil. 2008; 20 Suppl 1:8–19. [PubMed: 18402638]

Cobine CA, Hennig GW, Bayguinov YR, Hatton WJ, Ward SM, Keef KD. Interstitial cells of Cajal in the cynomolgus monkey rectoanal region and their relationship to sympathetic and nitrergic nerves. Am J Physiol Gastrointest Liver Physiol. 2010a; 298:G643–G656. [PubMed: 20150245]

Cobine CA, Duffy AM, Yan W, Ward SM, Sanders KM, Keef KD. Comparison of the morphological and functional properties of the internal anal sphincter in wild type mice (C57BL/6) and mice containing the reduced function Kit allele (Wv). Neurogastroenterol Motil. 2010b; 22 Suppl 1:86.

Farre R, Wang XY, Vidal E, Domenech A, Pumarola M, Clave P, Huizinga JD, Jimenez M. Interstitial cells of Cajal and neuromuscular transmission in the rat lower oesophageal sphincter. Neurogastroenterol Motil. 2007; 19:484–496. [PubMed: 17564630]

Fujita A, Takeuchi T, Jun H, Hata F. Localization of Ca^{2+}-activated K^+ channel, SK3, in fibroblast-like cells forming gap junctions with smooth muscle cells in the mouse small intestine. J Pharmacol Sci. 2003; 92:35–42. [PubMed: 12832853]

Goyal RK, Chaudhury A. Mounting evidence against the role of ICC in neurotransmission to smooth muscle in the gut. Am J Physiol Gastrointest Liver Physiol. 2010; 298:G10–G13. [PubMed: 19892937]

Hamilton TG, Klinghoffer RA, Corrin PD, Soriano P. Evolutionary divergence of platelet-derived growth factor alpha receptor signaling mechanisms. Mol Cell Biol. 2003; 23:4013–4025. [PubMed: 12748302]

Harvey N, McDonnell B, McKechnie M, Keef KD. Role of L-type calcium channels, membrane potential and nitric oxide in the control of myogenic activity in the primate internal anal sphincter. Gastroenterology. 2008; 134:A63.

Hashitani H, Suzuki H. Properties of spontaneous Ca^{2+} transients recorded from interstitial cells of Cajal-like cells of the rabbit urethra in situ. J Physiol (Lond). 2007; 583:505–519. [PubMed: 17615099]

Horiguchi K, Komuro T. Ultrastructural observations of fibroblast-like cells forming gap junctions in the W/W(nu) mouse small intestine. J Auton Nerv Syst. 2000; 80:142–147. [PubMed: 10785280]

Huizinga JD, Zarate N, Farrugia G. Physiology, injury, and recovery of interstitial cells of Cajal: basic and clinical science. Gastroenterology. 2009; 137:1548–1556. [PubMed: 19778538]

Iino S, Nojyo Y. Immunohistochemical demonstration of c-Kit-negative fibroblast-like cells in murine gastrointestinal musculature. Arch Histol Cytol. 2009; 72:107–115. [PubMed: 20009347]

Iino S, Horiguchi K, Nojyo Y. Interstitial cells of Cajal are innervated by nitrergic nerves and express nitric oxide-sensitive guanylate cyclase in the guinea-pig gastrointestinal tract. Neuroscience. 2008; 152:437–448. [PubMed: 18280665]

Iino S, Horiguchi K, Horiguchi S, Nojyo Y. c-Kit-negative fibroblast-like cells express platelet-derived growth factor receptor alpha in the murine gastrointestinal musculature. Histochem Cell Biol. 2009a; 131:691–702. [PubMed: 19280210]

Iino S, Horiguchi K, Nojyo Y, Ward SM, Sanders KM. Interstitial cells of Cajal contain signalling molecules for transduction of nitrergic stimulation in guinea pig caecum. Neurogastroenterol Motil. 2009b; 21:542–543. [PubMed: 19175750]

Klemm MF, Lang RJ. Distribution of Ca^{2+}-activated K^{+} channel (SK2 and SK3) immunoreactivity in intestinal smooth muscles of the guinea-pig. Clin Exp Pharmacol Physiol. 2002; 29:18–25. [PubMed: 11906457]

Komuro T. Comparative morphology of interstitial cells of Cajal: ultrastructural characterization. Microsc Res Tech. 1999; 47:267–285. [PubMed: 10602287]

Kurahashi M, Niwa Y, Cheng J, Ohsaki Y, Fujita A, Goto H, Fujimoto T, Torihashi S. Platelet-derived growth factor signals play critical roles in differentiation of longitudinal smooth muscle cells in mouse embryonic gut. Neurogastroenterol Motil. 2008; 20:521–531. [PubMed: 18194151]

Kurahashi M, Zheng H, Dwyer L, Ward SM, Koh SD, Sanders KM. A functional role for the “fibroblast-like cells” in gastrointestinal smooth muscles. J Physiol (Lond). 2011; 589:697–710. [PubMed: 21173079]

Kwon JG, Hwang SJ, Hennig GW, Bayguinov Y, McCann C, Chen H, Rossi F, Besmer P, Sanders KM, Ward SM. Changes in the structure and function of ICC networks in ICC hyperplasia and gastrointestinal stromal tumors. Gastroenterology. 2009; 136:630–639. [PubMed: 19032955]

Lavoie B, Balemba OB, Nelson MT, Ward SM, Mawe GM. Morphological and physiological evidence for interstitial cell of Cajal-like cells in the guinea pig gallbladder. J Physiol (Lond). 2007; 579:487–501. [PubMed: 17204499]

Lee HT, Hennig GW, Fleming NW, Keef KD, Spencer NJ, Ward SM, Sanders KM, Smith TK. The mechanism and spread of pacemaker activity through myenteric interstitial cells of Cajal in human small intestine. Gastroenterology. 2007; 132:1852–1865. [PubMed: 17484879]

de, Lorijn F.; de, Jonge WJ.; Wedel, T.; Vanderwinden, JM.; Benninga, MA.; Boeckxstaens, GE. Interstitial cells of Cajal are involved in the afferent limb of the rectoanal inhibitory reflex. Gut. 2005; 54:1107–1113. [PubMed: 16009682]

McDonnell B, Hamilton R, Fong M, Ward SM, Keef KD. Functional evidence for purinergic inhibitory neuromuscular transmission in the mouse internal anal sphincter. Am J Physiol Gastrointest Liver Physiol. 2008; 294:G1041–G1051. [PubMed: 18308858]

Mutafova-Yambolieva VN, O'Driscoll K, Farrelly A, Ward SM, Keef KD. Spatial localization and properties of pacemaker potentials in the canine rectoanal region. Am J Physiol Gastrointest Liver Physiol. 2003; 284:G748–G755. [PubMed: 12540368]

Rattan S. The internal anal sphincter: regulation of smooth muscle tone and relaxation. Neurogastroenterol Motil. 2005; 17 Suppl 1:50–59. [PubMed: 15836455]

Rumessen JJ, Thuneberg L. Plexus muscularis profundus and associated interstitial cells. I. Light microscopical studies of mouse small intestine. Anat Rec. 1982; 203:115–127. [PubMed: 6179440]

Rumessen JJ, Thuneberg L. Interstitial cells of Cajal in human small intestine. Ultrastructural identification and organization between the main smooth muscle layers. Gastroenterology. 1991; 100:1417–1431. [PubMed: 2013387]

Sanders KM, Hwang SJ, Ward SM. Neuroeffector apparatus in gastrointestinal smooth muscle organs. J Physiol (Lond). 2010; 588:4621–4639. [PubMed: 20921202]

Sang Q, Young HM. Chemical coding of neurons in the myenteric plexus and external muscle of the small and large intestine of the mouse. Cell Tissue Res. 1996; 284:39–53. [PubMed: 8601295]

Sergeant GP, Large RJ, Beckett EA, McGeough CM, Ward SM, Horowitz B. Microarray comparison of normal and W/Wv mice in the gastric fundus indicates a supersensitive phenotype. Physiol Genomics. 2002; 11:1–9. [PubMed: 12361985]

Terauchi A, Kobayashi D, Mashimo H. Distinct roles of nitric oxide synthases and interstitial cells of Cajal in rectoanal relaxation. Am J Physiol Gastrointest Liver Physiol. 2005; 289:G291–G299. [PubMed: 15845873]

Vanderwinden JM, Rumessen JJ, De Laet MH, Vanderhaeghen JJ, Schiffmann SN. CD34+ cells in human intestine are fibroblasts adjacent to, but distinct from, interstitial cells of Cajal. Lab Invest. 1999; 79:59–65. [PubMed: 9952111]

Vanderwinden JM, Rumessen JJ, De Laet MH, Vanderhaeghen JJ, Schiffmann SN. CD34 immunoreactivity and interstitial cells of Cajal in the human and mouse gastrointestinal tract. Cell Tissue Res. 2000; 302:145–153. [PubMed: 11131126]

Vanderwinden JM, Rumessen JJ, de Kerchove DA Jr, Gillard K, Panthier JJ, De Laet MH, Schiffmann SN. Kit-negative fibroblast-like cells expressing SK3, a Ca^{2+}-activated K^{+} channel, in the gut musculature in health and disease. Cell Tissue Res. 2002; 310:349–358. [PubMed: 12457234]

Wang XY, Alberti E, White EJ, Mikkelsen HB, Larsen JO, Jimenez M, Huizinga JD. Igf1r+/CD34+ immature ICC are putative adult progenitor cells, identified ultrastructurally as fibroblast-like ICC in Ws/Ws rat colon. J Cell Mol Med. 2009; 13:3528–3540. [PubMed: 19220583]

Ward SM, Sanders KM. Involvement of intramuscular interstitial cells of Cajal in neuroeffector transmission in the gastrointestinal tract. J Physiol 576 (Lond). 2006:675–682.

Ward SM, Burns AJ, Torihashi S, Sanders KM. Mutation of the proto-oncogene c-kit blocks development of interstitial cells and electrical rhythmicity in murine intestine. J Physiol (Lond). 1994; 480:91–97. [PubMed: 7853230]

Ward SM, Morris G, Reese L, Wang XY, Sanders KM. Interstitial cells of Cajal mediate enteric inhibitory neurotransmission in the lower esophageal and pyloric sphincters. Gastroenterology. 1998; 115:314–329. [PubMed: 9679037]

Ward SM, Beckett EA, Wang X, Baker F, Khoyi M, Sanders KM. Interstitial cells of Cajal mediate cholinergic neurotransmission from enteric motor neurons. J Neurosci. 2000; 20:1393–1403. [PubMed: 10662830]

Yoneda S, Fukui H, Takaki M. Pacemaker activity from submucosal interstitial cells of Cajal drives high-frequency and low-amplitude circular muscle contractions in the mouse proximal colon. Neurogastroenterol Motil. 2004; 16:621–627. [PubMed: 15500519]

Zhang Y, Carmichael SA, Wang XY, Huizinga JD, Paterson WG. Neurotransmission in lower esophageal sphincter of W/Wv mutant mice. Am J Physiol Gastrointest Liver Physiol. 2010; 298:G14–G24. [PubMed: 19850967]

Zhou DS, Komuro T. Interstitial cells associated with the deep muscular plexus of the guinea-pig small intestine, with special reference to the interstitial cells of Cajal. Cell Tissue Res. 1992; 268:205–216. [PubMed: 1617694]

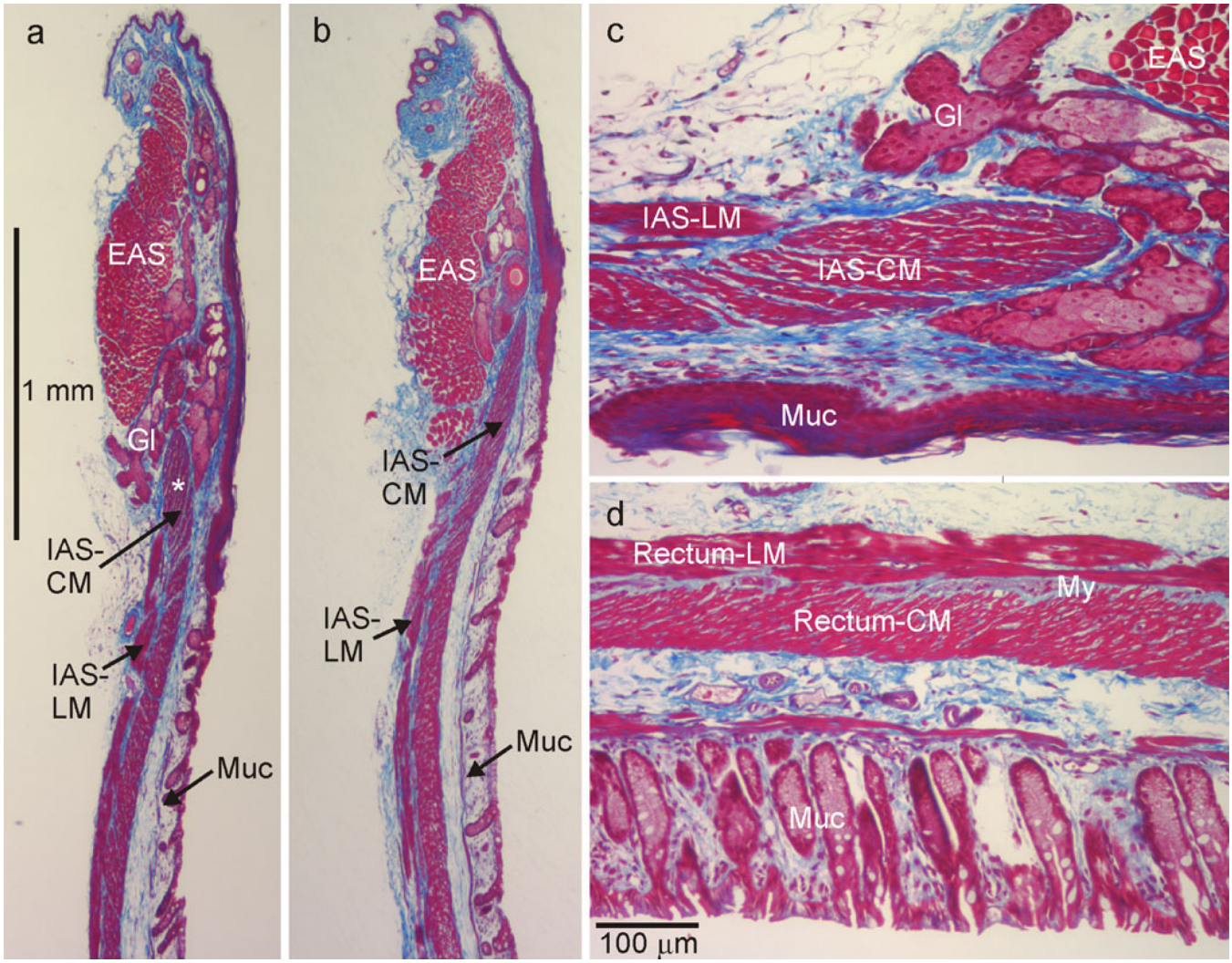

Fig. 1.

Morphological features of the mouse rectoanal region. Masson's Trichrome staining techniques were used to identify muscular (*red/pink*) and connective tissue (*blue*) structures in 10-µm-thick microtome sections. Circular muscle (*CM*) and longitudinal muscle (*LM*) layers of the internal anal sphincter (*IAS*) were visible, although the former extended more distally than the latter (**a–c**). The external anal sphincter (*EAS*) was located distal to the IAS with some overlap between these sphincters (**b**). Occasionally, secretory glands (*Gl*) were interposed between the IAS and EAS (**a,c**) and drained into the gut lumen (outlet not shown). The mucosa (*Muc*) was apparent at the lumenal edge of each image (**a–d**). **c** Higher magnification image of a region in **a** (*star*) rotated 90° clockwise. **d** Section from the rectum (4 mm from the anal verge) at the same magnification. The connective tissue septa in the CM layer of the IAS (**c**) are thicker than in the rectum (**d**). CM and LM layers are separated by connective tissue at the myenteric (*My*) surface of the IAS (**c**) and rectum (**d**). During fixation, muscles were stretched in the longitudinal but not the transverse direction leading to some distortion in the orientation of CM fibers

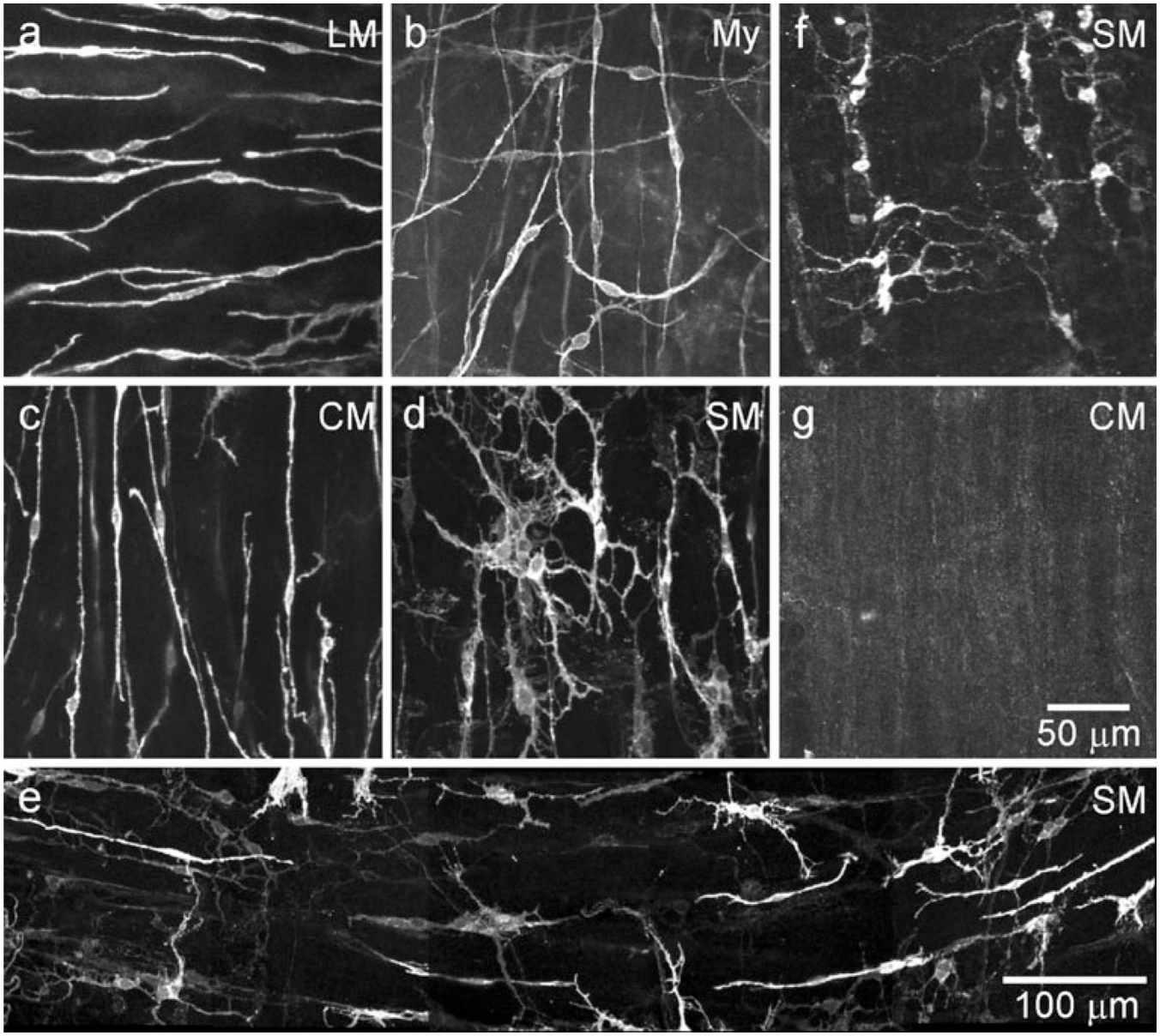

Fig. 2.

Spindle-shaped intra-muscular ICC (ICC-IM) and stellate-shaped submucosal ICC (ICC-SM) are present in the wild-type mouse IAS, whereas only ICC-SM persist in the *W/W*^{v}. Spindle-shaped longitudinal muscle (LM; **a**) and circular muscle (*CM*; **c**) ICC-IM are identified by immunohistochemical labeling of KIT. A distinct myenteric (*My*) network of ICC is not observed (**b**). A few ICC from either the LM layer (*horizontal*) or CM layer (*vertical*) can be seen, plus a single stellate-shaped ICC. Stellate-shaped ICC-SM are present along the submucosal (*SM*) surface (**d, e**) where they appear in clusters in this composite image (**e**) rather than forming a distinct network. ICC-SM persist in the *W/W*^{v} mouse (**f**), whereas ICC-IM are largely absent (**g**). Optical section thicknesses: **a** 10.5 μm, **b** 1.25 μm, **c** 12 μm, **d** 9.5 μm, **e** 7.5 μm, **f** 9.5 μm, **g** 6 μm

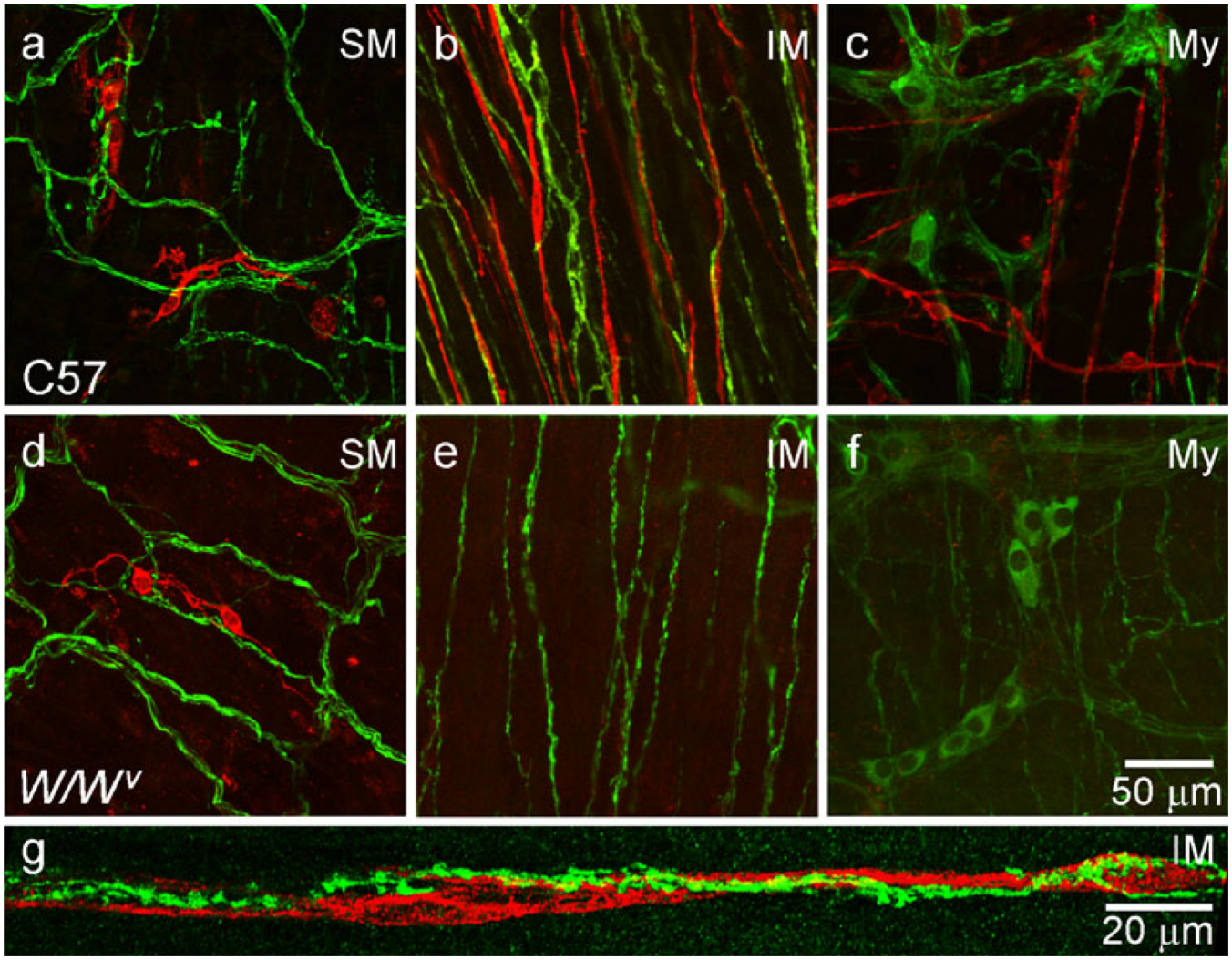

Fig. 3.

Some ICC-IM are closely associated with nNOS$^+$ nerve fibers in the IAS of the wild-type (WT, *C57*) mouse but not in the IAS of the *W/W^v* mouse. Dual-labeling of ICC (*red*) and nNOS$^+$ nerve fibers (*green*) in whole-mount preparations at various positions within the IAS. nNOS$^+$ nerve fibers form a plexus at the submucosal (*SM*, **a, d**) and myenteric (*My*, **c, f**) surfaces of WT and *W/W^v* mice. Clusters of submucosal ICC (ICC-SM, *red*) can be seen in WT and *W/W^v* mice (**a, d**). Intramuscular (*IM*) nNOS$^+$ nerve fibers run parallel to smooth muscle cells in WT (**b, g**) and *W/W^v*(**e**) mice. A network of stellate-shaped myenteric (*My*) ICC is not observed in either WT or *W/W^v* (**c, f**). Some ICC-IM are closely associated with these nerves in the WT (**b**) but not the *W/W^v* mouse (**e**). **g** Higher magnification image showing varicose nNOS$^+$ nerve fibers closely associated with ICC-IM in a WT mouse IAS. Optical section thicknesses: **a** 2 µm, **b** 6.75 µm, **c** 10 µm, **d** 6.5 µm, **e** 7.5 µm, **f** 5 µm, **g** 2.9 µm

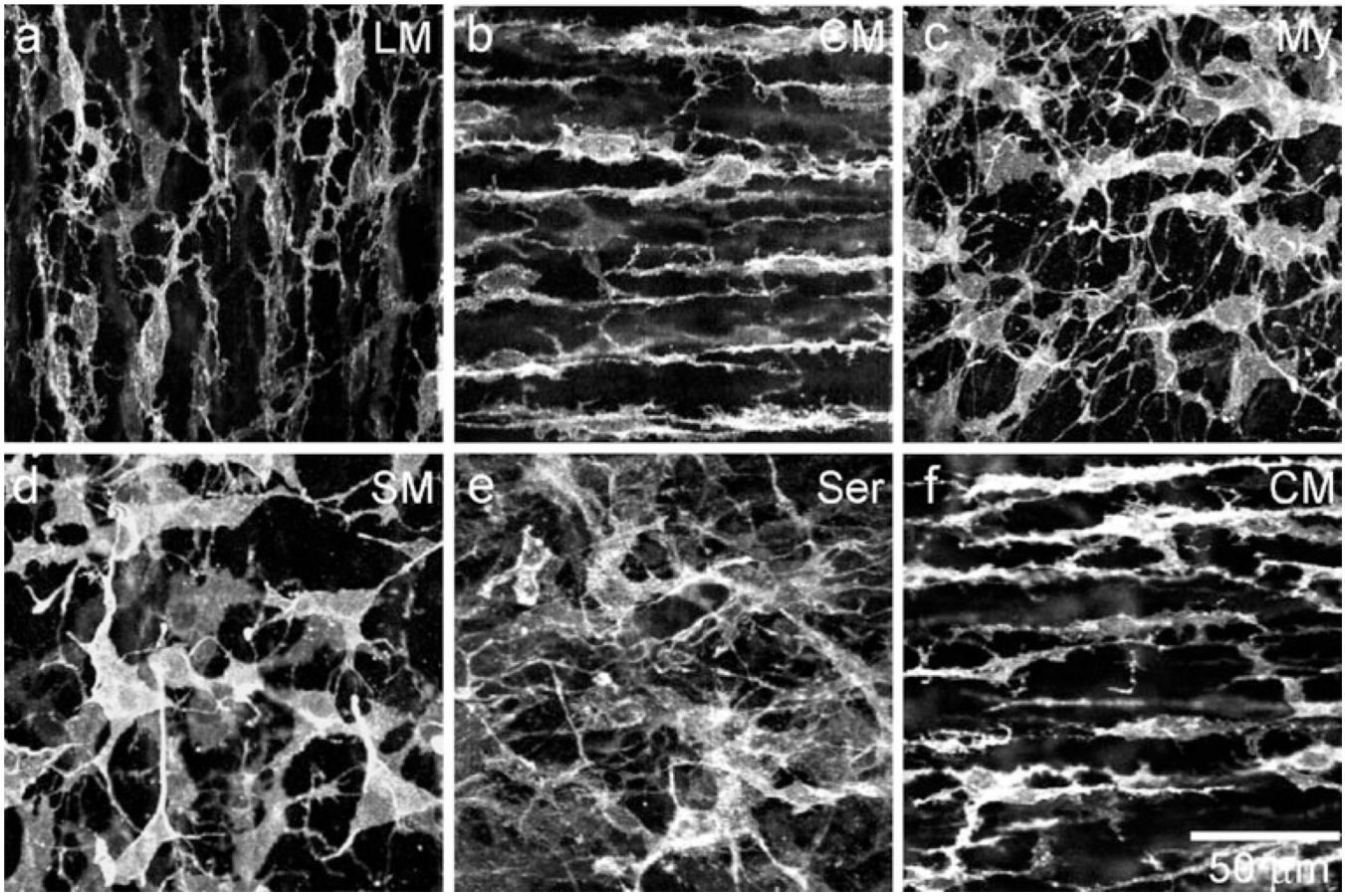

Fig. 4.

Various populations of PDGFRα$^+$ cells are found within the mouse IAS. Intramuscular PDGFRα$^+$ cells (PDGFRα$^+$-IM) are found within the LM (**a**) and CM (**b, f**) running parallel to the long-axis of smooth muscle cells (*SMC*) in the wild-type (*C57*) and *W/W^v* mouse IAS. PDGFRα$^+$ cells are also found along the myenteric surface (*My*, **c**), within the submucosa (*SM*, **d**) and along the serosal surface (*Ser*, **e**). Optical section thicknesses: **a** 2 µm, **b** 1.75 µm, **c** 2.5 µm, **d** 1.5 µm, **e** 3.5 µm, **f** 2 µm

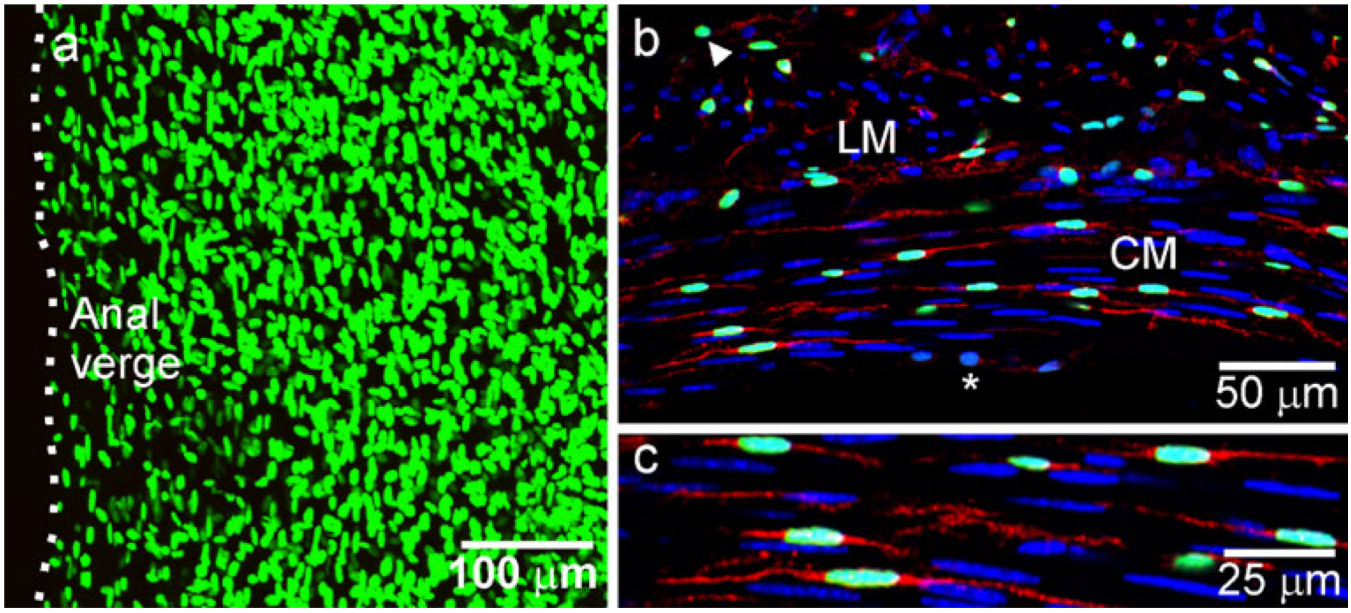

Fig. 5.

PDGFRα^{+} cells are abundant throughout the IAS of the *Pdgfra$^{tm11(eGFP)Sor}$/J* heterozygote mouse. **a** Cells expressing eGFP (*green*) are observed throughout the muscularis of a whole-mount preparation of the IAS from the *Pdgfra$^{tm11(eGFP)Sor}$/J* heterozygote mouse (*dotted line* distal most extremity of the IAS or *Anal verge*). **b, c** Transverse cryostat section showing eGFP-expressing cells in the longitudinal (*LM*) and circular (*CM*) muscle layers. eGFP-expressing cells are confirmed to be PDGFRα^{+} by immunohistochemical labeling techniques (*red*). Supplementary Fig. 2 reveals that eGFP is present even in PDGFRα^{+} cells with predominantly blue labeling in the cell body (*star*) and that eGFP^{+} cell bodies in the LM layer (*triangle*) also label with PDGFRα. All cells present are identified with the nuclear stain DAPI (*blue*) in the IAS. **c** Higher magnification of **b** *bottom left* (slightly rotated). Optical section thicknesses: **a** 49 μm, **b** 9 μm, **c** 9 μm

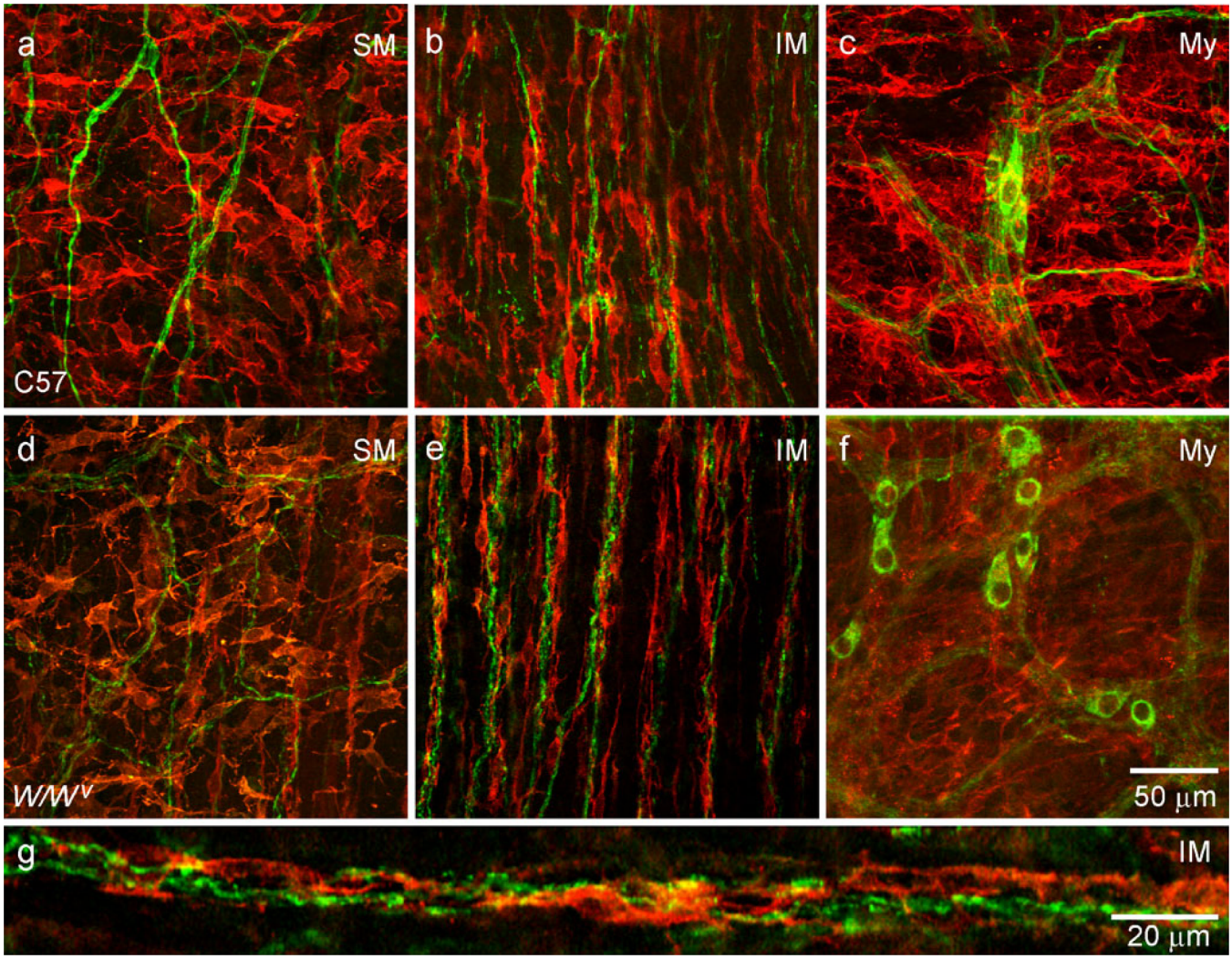

Fig. 6.

PDGFRα$^+$-IM are closely associated with nNOS$^+$ nerve fibers in the WT and *W/W*^{v} mouse IAS. Dual-labeling of PDGFRα$^+$ cells (*red*) and nNOS$^+$ nerve fibers (*green*) in whole-mount preparations within the IAS. PDGFRα$^+$ cells form a network along the submucosal (*SM*, **a, d**) and myenteric (*My*, **c,f**) surfaces but these cells do not appear to be highly associated with nNOS$^+$ nerve fibers. In contrast, intramuscular (*IM*) nNOS$^+$ nerve fibers are closely aligned with PDGFRα$^+$ cells (**b, e**). **g** Higher magnification image showing varicose nNOS$^+$ nerve fibers closely aligned with PDGFRα$^+$-IM. Optical section thicknesses: **a** 2 μm, **b** 2.5 μm, **c** 4 μm, **d** 2 μm, **e** 1.5 μm, **f** 3.5 μm, **g** 1.5 μm

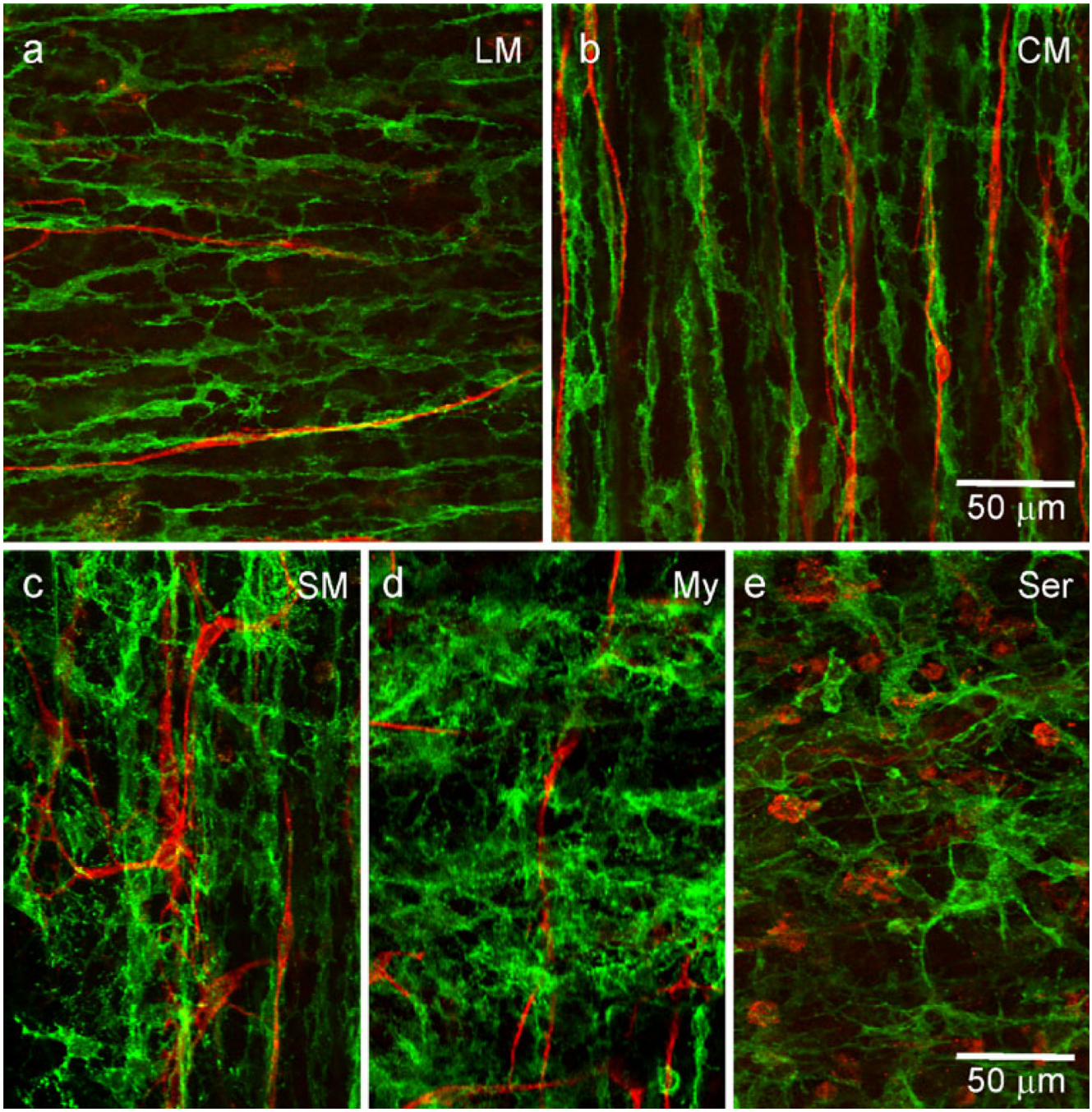

Fig. 7.

PDGFRα$^+$ cells are closely associated with ICC-IM in WT mouse IAS. Dual-labeling of PDGFRα$^+$ cells (*green*) and ICC (*red*) in whole-mount preparations of the IAS of the WT mouse. ICC-IM are closely associated with PDGFRα$^+$-IM in the LM (**a**) and CM (**b**) layers. In contrast, ICC located near the submucosal (*SM*, **c**) and myenteric (*My*, **d**) surfaces appear to have little relationship to PDGFRα$^+$ cells. Round KIT$^+$ cells seen within the serosa (*Ser*, **e**) are likely to be mast cells and do not appear to have a close association with PDGFRα$^+$ cells. Optical section thicknesses: **a** 2.5 µm, **b** 3 µm, **c** 5.5 µm, **d** 2.5 µm, **e** 3.5 µm

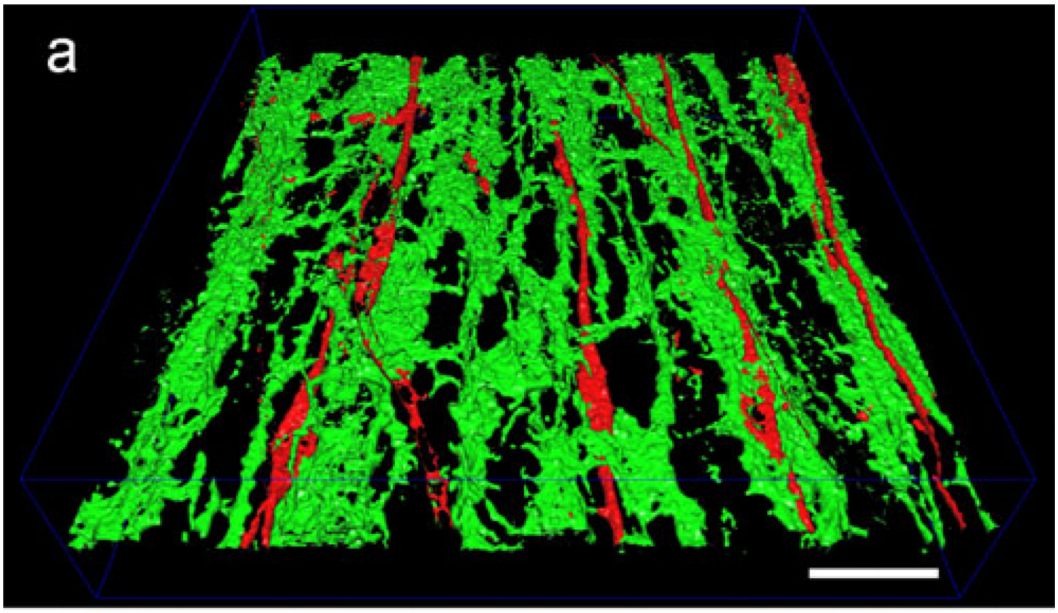

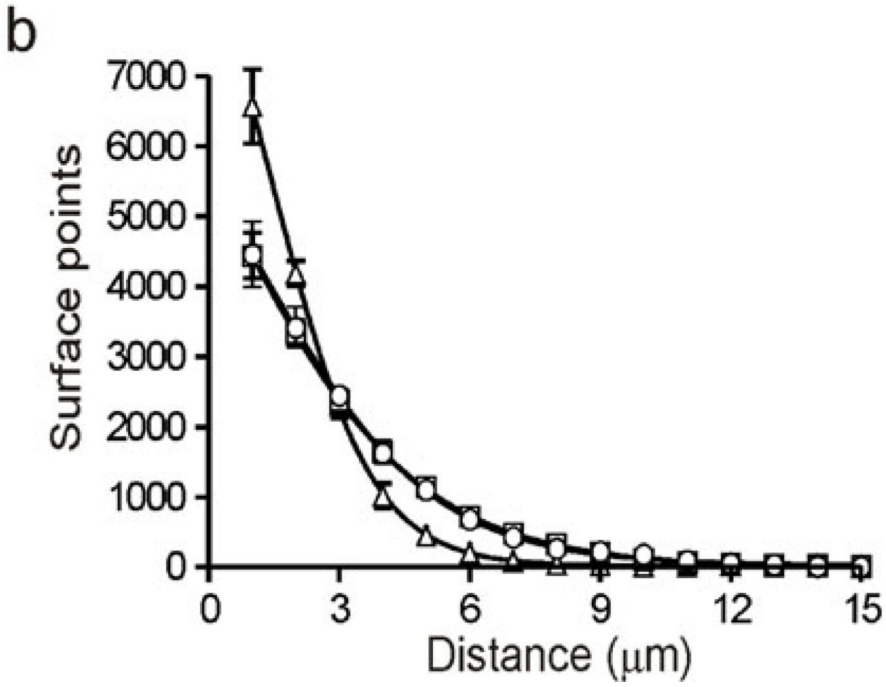

Fig. 8.

Alignment of ICC-IM, PDGFRα$^+$-IM and nNOS$^+$ nerve fibers determined by using a minimum surface distance algorithm. Alignment between cell types was evaluated by first generating three-dimensional surface reconstructions from dual-labeled preparations (see Kwon et al. 2009; Cobine et al. 2010a). **a** Example of one of these reconstructions for ICC-IM (*red*) and PDGFRα$^+$-IM (*green*) in a WT mouse IAS image (8.75-μm-thick optical section; see also Supplementary Fig. 4). *Bar* 20 μm. **b** The relationship of one cell-type to the other was determined by the application of a minimum surface distance algorithm to these surface reconstructions. The resulting number of surface points separated by each distance was then plotted. The greatest number of ICC-IM surface points was found to be≤1

μm from PDGFRα$^+$-IM surface points (*triangles*; ~6,500 out of 15,000 randomly sampled surface points), with the maximum distance between the two cell types being≤8 μm. The relationship of nNOS$^+$ nerve fibers to ICC-IM (*squares*) and PDGFRα$^+$-IM (*circles*) was similar, with the greatest number of surface points (~4,500) again being found to be≤1 μm, whereas the maximum distance between surface points was≤11 μm. The mean value for PDGFRα$^+$-IM/ICC-IM at≤1 μm was significantly greater than that for either PDGFRα$^+$-IM/nNOS or ICC-IM/nNOS

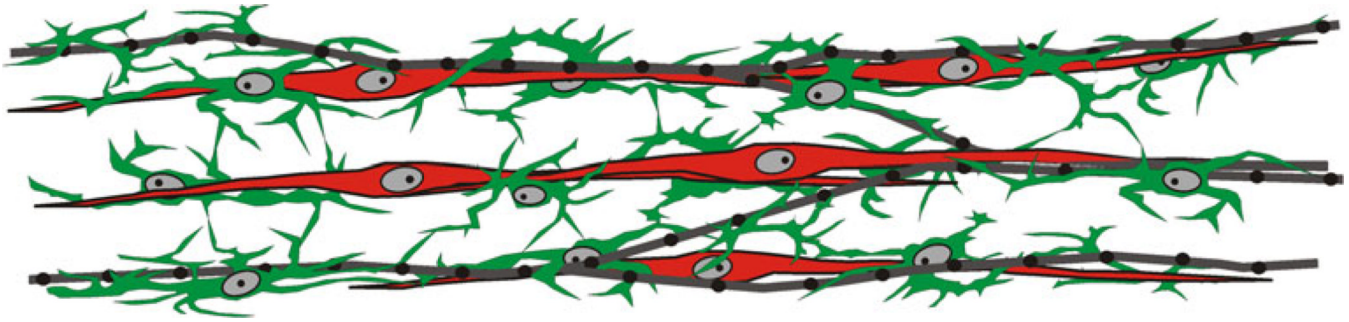

Fig. 9.

Representation of the overall relationship of ICC-IM and PDGFRα$^+$-IM to nitrergic nerves in the mouse IAS. The morphology of ICC-IM (*red*) and PDGFRα$^+$-IM (*green*) differed from one another. ICC-IM are long spindle-shaped cells, whereas PDGFRα$^+$-IM are shorter, are highly branched and appear to form a loosely connected network (see also Fig. 8). Nitrergic nerves (*gray*, *black*) are generally aligned parallel to the circular muscle, ICC-IM and PDGFRα$^+$-IM. All nerves and ICC-IM are accompanied by PDGFRα$^+$-IM (see Figs. 6, 7). ICC-IM are also accompanied by nerves but often not over their entire length (Fig. 3). Since ICC-IM and nitrergic nerves are always accompanied by PDGFRα$^+$-IM, many regions are likely to occur in which all three structures are co-localized

Table 1

Primary antibodies

Primary antibody	Source	Monoclonal or polyclonal	Host	Antigen	Specificity	Working dilution
Anti-mSCFR	R&D Systems, Minneapolis, Minn., USA	Poly	Goat	Extracellular domain of stem cell factor receptor	Specifically recognizes mouse SCFR with Western blot and ELISA	1:1000
Anti-KIT (ACK2)	Gibco BRL, Gaithersburg, Md., USA	Mono	Rat	Extracellular domain of the c-*kit* proto-oncogene	Recognizes two bands at 120 and 160 kDa corresponding to KIT in murine mast cell extract with Western blot	1:1000
Anti-PDGFRα	eBioscience, San Diego, Calif. USA	Mono	Rat	α Chain of the platelet-derived growth factor receptor	Recognizes mouse CD140a, the α chain of the platelet-derived growth factor receptor	1:500
Anti-PDGFRα	R&D Systems	Poly	Goat	Extracellular domain of mouse platelet-derived growth factor receptor α	Neutralizes mouse PDGFRα bioactivity	1:1000
Anti-nNOS	Gift from Dr. Piers Emson, Mol. Sci. Group, Cambridge, UK	Poly	Sheep	Neuronal isoform of nitric oxide synthase (nNOS)	Detects neuronal isoform of nitric oxide synthase (nNOS) in central and peripheral nitrergic neurons	1:1000
Anti-NOS1 (R-20)	Santa Cruz Biotechnology, Santa Cruz, Calif., USA	Poly	Rabbit	Epitope near the c-terminus of NOS1	Recognizes NOS1 (ncNOS)	1:500